AUTOMATIC NON-PARAMETRIC CAPSID SEGMENTATION USING WAVELETS TRANSFORM AND GRAPH

Florian Levet[1,2,3], *Aurélia Cassany*[6,7], *Michael Kann*[6,7,8], *Jean-Baptiste Sibarita*[4,5]

(1) Univ. Bordeaux, Bordeaux Imaging Center, F-33000 Bordeaux, France
(2) CNRS, Bordeaux Imaging Center, UMS 3420, F-33000 Bordeaux, France
(3) INSERM, Bordeaux Imaging Center, US 04, F-33000 Bordeaux, France
(4) Univ. Bordeaux, IINS, UMR 5297, F-33000 Bordeaux, France
(5) CNRS, IINS, UMR 5297, F-33000 Bordeaux, France
(6) Univ. Bordeaux, FMP, UMR 5234, F-33000 Bordeaux, France
(7) CNRS, FMP, UMR 5234, F-33000 Bordeaux, France
(8) Bordeaux University Hospital, Department of Virology, F-33000 Bordeaux, France

ABSTRACT

Every year, one million people dies from Hepatitis B virus. As for other viruses, its genetic material is enclosed by a capsid whose segmentation and classification is essential. In this paper, we present a novel capsid segmentation technique which is a combination of a "à trous" wavelet process (for background filtering) and a graph-based structure (for segmentation and classification). Capsids were acquired in transmission electron microscopy (TEM) as a set of 9 series of 40 images each. Our technique achieved as much as 80% of capsid detection and classification for 8 of the series, reaching more than 90% for 5 of them.

Index Terms— Capsid, image processing, "à trous" wavelet, segmentation, skeletization, graph-based structure

1. INTRODUCTION

Hepatitis B virus (HBV) is a major human pathogen, which is responsible of approximately one million of deaths each year. Chronically HBV infected patients can develop liver cirrhosis and primary hepatocellular carcinoma. HBV is a small enveloped virus which encloses an icosahedral capsid and a partially double stranded circular DNA genome. The capsid is composed by 240 copies (T=4 arrangements) or 180 copies (T=3 arrangements) of a single protein species termed core protein or capsid protein. Core proteins clustered into dimers generate 120 or 90 spikes on the surface of the shell. These two organizations of icosahedral capsid are found in recombinant capsids from *E.coli* [1] as well as in the liver and in the virion from HBV infected patients [2], but the role of these forms remains unknown. The T=3 forms is supposed to be less stable than T=4.

Electron microscopy and X-ray crystallography studies have shown than 10-20% of particles assemble in small particle (T=3) rather than in larger particle (T=4) upon bacterial expression and in native virions [3, 4]. Recent analysis using an automatic particle finding program revealed that cores from virions were almost exclusively (98%) of the T=4 size [5]. When the measurement is done across the tips of the spikes, average radius of T=4 capsids is close to 18nm while it is close to 16nm for the T=3 ones [1].

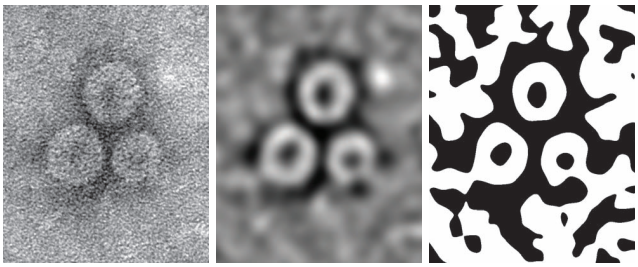
Segmenting and classifying the different capsids is essential to finally determine what their specific role is for HBV or other viruses [6]. Since the size difference between the T=4 and T=3 capsids is relatively small, an automatic tool is needed to avoid introducing bias by human quantification. In this paper, we propose an automatic and non-parametric segmentation method which classifies capsids into T=3 or T=4 type. It combines i) "à trous" wavelets transform [7] as a preprocessing step to binarize the original image, ii) skeletization and iii) graph theory algorithms to identify the capsids from the binarized image.

2. IMAGE ACQUISITION

Original images were obtained by a transmission electron microscope (TEM) at 80kV using high resolution mode (H7650, HITACHI). Images were taken at X300,000 magnification and have a resolution of 0.179nm/pixel. Capsids are defined as small regular circular objects with a radius of 17 nm, $\pm$ 3.5nm. They appear in TEM images as bright objects with a radius close to 100 pixels as illustrated in Figure 1.

3. "A TROUS" WAVELETS SEGMENTATION

The idea of the method is first to binarize the original image in order to identify the capsids. Common segmentation or filtering techniques such as basic thresholding or unsharp



(a) (b) (c)

Fig. 1. (a) Original EM image. (b) Image obtained from the 6th wavelet coefficient subband. (c) Wavelet segmentation.

masking are not adapted because of the important size of the capsids and the poor contrast and SNR of TEM images. We used wavelets as a suitable segmentation tool, thanks to their intrinsic multiresolution properties.

Wavelets transform are widely used to perform image processing and analysis. The "à trous" algorithm represents a discrete approach to the classical continuous wavelet transform [7]. Similarly to the fast discrete wavelet transform, the input signal is analyzed by using the coefficients of a properly chosen low-pass filter. While in biorthogonal wavelets the output is subsampled, in the "à trous" case the filter is "stretched" to take into account the rescaling and the convolution is performed without any subsampling. Usually, the chosen low-pass filter is a B_3 spline.

We define $c_0(k)$ as the original EM image. The smoothed data $c_i(k)$ at a given resolution i and at pixel k is obtained by the convolution $c_i(k) = \sum_l h(l)c_{i-1}(k + 2^{i-1}l)$, where h is the low-pass scaling function. The difference between two consecutive resolution levels $w_i(k) = c_{i-1}(k) - c_i(k)$ represents the wavelet coefficients at level i. Then, it is sufficient to directly work on the wavelet coefficients to perform image processing or segmentation [8].

A common problem is to choose a correct threshold. In microscopy with CDD camera, the noise is a mixture of Gaussian (electronic) and Poisson (photons) ones []. Thus, an image I can be defined as $I = A + \epsilon$ where A is the noiseless image and ϵ the noise. During the wavelet transform, the noise ϵ is decomposed in all of the wavelet subbands, which means that a different part of the noise is found in each subband. Nevertheless, more than 80% of the noise is present in the first wavelet plane.

To determine the threshold value needed to segment the staining clusters, an estimation of the noise variance σ_ϵ has to be computed. [9] proposed a robust estimation of noise level $\hat{\sigma}_\epsilon$ based on the median absolute value of the wavelet coefficients as :

$$\hat{\sigma}_\epsilon = \frac{median(|w_1(x,y)|)}{0.06745}$$

where $w_1(x,y)$ is the first coefficient subband of the "à trous" wavelets. Since most of the noise ϵ is part of w_1 while containing little useful signal, such estimator has become very popular and is widely used.

For $w_l(x,y)$, a coefficient of the wavelet subband l, we define $\overline{w_l(x,y)}$ as the mean of $w_l(x,y)$ with its rank 1 neighbors. The signal at $w_l(x,y)$ is computed as :

$$s_l(x,y) = \sqrt{\left|\overline{w_l(x,y)} - \hat{\sigma}_\epsilon^2\right|}$$

If $s_l(x,y) < \hat{\sigma}_\epsilon$ (resp. $\geq$), $w_l(x,y)$ is tagged as a background (resp. object) pixel. Note that we use the 6th wavelet coefficients subband to perform this segmentation because the size of the corresponding convolution is close to the capsid size.

Figure 1(a) is the image before segmentation. The signal image of the 6th wavelet coefficient subband is shown in Figure 1(b). It is a blurred version of the original one with enhanced contrast. Unfortunately, this signal image tends to create artefact structures in the background too, leading to the segmentation of unwanted background alongside the capsids (see Figure 1(c)).

4. CAPSID IDENTIFICATION

After wavelet segmentation, capsids are represented by a white circular ring. Nevertheless, two cases happen as illustrated in Figure 1(c). (1) The capsid stands alone with no other object close to it. (2) The capsid is surrounded by others or by non specific background. In the second case, the objects need to be further processed to be cut and identified.

4.1. Stand-alone capsid identification

Applicable stand-alone capsids are objects having an area between 450 nm^2 (2500 pixels^2) and 1800 nm^2 (10100 pixels^2).

If the object area fits these requirements, its contour is converted into a Catmull-Rom spline [10], which provides a C^1-continuous interpolation of its control points. To get a spatial distribution of sample points as regular as possible along the contour, we perform an arc-length parametrization [10] of the spline which offers a much better accuracy for the points curvature. A relevant curvature is essential to compute the ellipse approximating the object contour by least-square fitting [11, 12]. Features such as orientation, axis length or circularity are then determined from the ellipse fitting. Finally, an object is tagged as capsid if its circularity (ratio between the small and large axis) is bigger than 0.8 (see Figure 2(b)).

4.2. Aggregated capsids identification

First, all identified stand-alone capsids are removed from the binarized image. Then, each remaining object is reduced to a skeleton, the latter being used to create the graph representation.

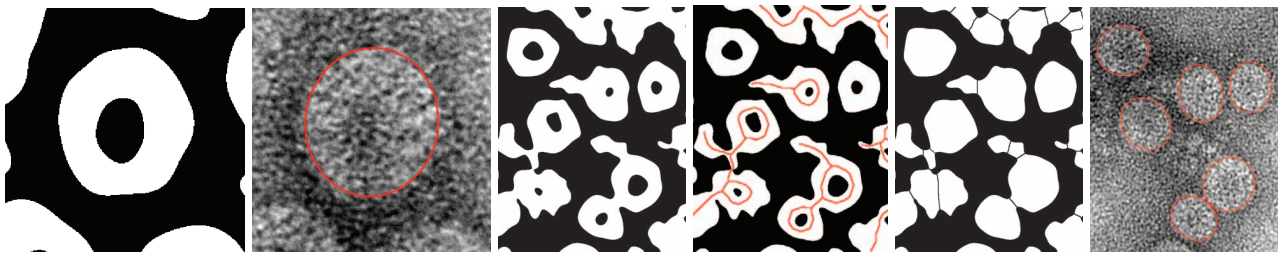


Fig. 2. (a) Binarization of a stand-alone capsid. (b) Corresponding ellipse approximation. (c) Binarization of aggregate capsids. (d) Corresponding skeletons after identification of stand-alone capsids. (e) Cutting of the aggregates by a watershed process. (f) Final capsids identification (stand-alone and aggregates)

4.2.1. Skeletonization

Thinning algorithms (e.g. [14]) generate skeletons which preserve the shape topologies. However, they are noise-sensitive and usually yield unwanted edges. In our case, this is not a problem since even a raw representation of the skeleton is sufficient to generate the graph representation. To speed-up the process, we use a parallel approach [13].

For each boundary pixel of the binary image, 8 thinning masks (see Figure 3(a)) are applied. In order to ensure a 1-pixel width skeleton, we introduce two retrieval masks (see Figure 3(b-c)) to the original approach [13]. If any of the thinning masks and none of the retrieval ones are matched, the pixel can be removed without losing the topology. Figure 2(d) shows the skeletonization of the binarized objects of the image. Objects with no skeleton were already identified as stand-alone capsids and removed before skeletonization.

4.3. Graph-based identification of capsids

Generating an undirected graph from a 1-pixel width skeleton is straightforward : we just have to browse the skeleton to generate its edges and vertices. Since capsids appear as white rings after wavelet filtering, they are represented by base cycles (cycles that can not be constructed by a union of other cycles) in the graph.

To localize the base cycles, the minimum spanning tree (MST) of the graph G has to be generated. The MST of G is the spanning tree which minimizes the weight of its edges (a spanning tree being a subgraph of G which is a tree and connects all the graph vertices together). In our implementation, we used the Kruskal's algorithm [15] to compute the MST of the graphs. Each edge of G that is not part of its MST adds a base cycle to G. We have then just to identify the edges that are part of this base cycle to identify the capsid position.

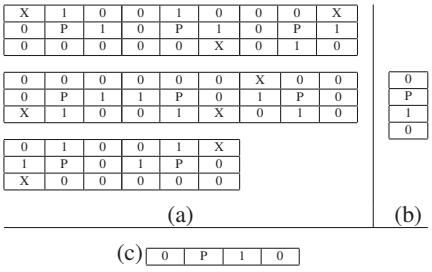


Fig. 3. (a)Thinning masks used in the technique of Ng et al. [13]. P is the pixel currently treated and X means that the value of the pixel may be 0 or 1. (b-c) Restoring masks added to ensure to have a 1-pixel width.

4.4. Final capsid identification

Since the positions of the aggregated capsids are determined, we need to separate them from the surrounding background objects or capsids to approximate their shape. A watershed process is applied on the binarized image to perform this cutting as illustrated in Figure 2(e). The capsid holes were filled before to avoid cutting the actual capsid shape (they are inside the skeletons represented by the base cycles). After this process, all capsids are stand-alone capsids and can be identified (see Figure 2(f)). Objects are then classified into two categories : capsids, which are objects with characteristics matching the specifications of Section 4.1 and candidates are objects with a circularity bigger than 0.65 and a radius between 11nm and 23nm (a candidate being an object that slightly does not fit the capsid requirements but may still be one).

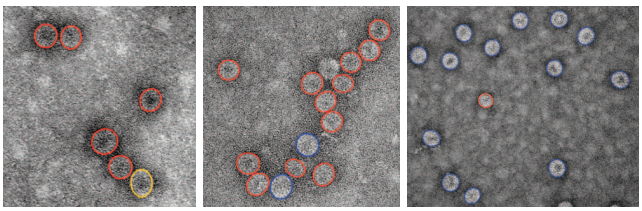


Fig. 4. Capsids segmented by the plugin. Three classes are displayed : T=3 capsids (red), T=4 capsids (blue) and candidates (orange).

5. RESULTS AND DISCUSSION

The software was developed in Java for ImageJ [16]. ImageJ is a powerful image processing system which is easy to extend by developing plugins. Emphasis was applied on the implementation of a user-friendly plugin. The plugin is directly used as a macro with no parameter. Besides, a mouse click can be used to change a candidate into a capsid and vice versa.

In this paper, we have presented an automatic non-parametric technique designed to segment and classify capsids. Starting from a binarization of the original image obtained with "à trous" wavelet filtering, a skeletization combined with graph-based algorithms is used to properly segment the capsids. Since T=3 capsids radius is close to 16nm while T=4 one is close to 18nm, we define the limit radius for the classification as 17nm. Figure 4 shows capsid segmentation performed by our plugin. T=3 capsids are underlined in red while T=4 capsids are blue and candidates are orange.

To test the robustness of our method, the plugin was used by a capsid specialist to determine the accuracy of the segmentation. The tests were done on 9 image series of capsids, each of one being composed of approximately 40 images. For each image, the number of detected capsids by the plugin is compared to the number detected by the user and normalized. Finally, a mean of these normalizations was done for each serie. As shown in Figure 5, we have detected more than 80% of the capsids for 8 of the series, this number reaching more than 90% for 5 of them. Besides, the ratio of T=3/T=4 capsids was 20% of T=3 capsids for 80% of the T=4 class which is equivalent to results obtained by other developped techniques [3, 4].

Acknowledgement

We thank Jessica Ragues for the expression and the purification of the capsids and Etienne Gontier and Sabrina Lacomme of the BIC for their image acquisition.

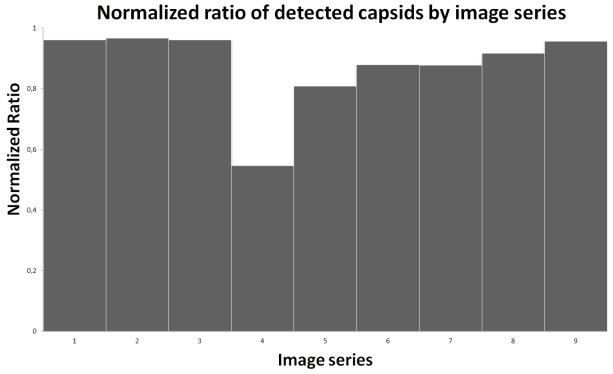


Fig. 5. Normalized ratio of detected capsids by the plugin versus detected capsids by the user. The ratio was determined by image series.

6. REFERENCES

[1] R.A. Crowther, N.A. Kiselev, B. Böttcher, J.A. Berriman, G.P. Borisova, V. Ose, and P. Pumpens, "Three-dimensional structure of hepatitis b virus core particles determined by electron cryomicroscopy," *Cell*, vol. 77, no. 6, pp. 943–950, 1994.

[2] J.M. Kenney, C.H. von Bonsdorff, M. Nassal, and S.D. Fuller, "Evolutionary conservation in the hepatitis b virus core structure : comparison of human and duck cores," *Structure*, vol. 3, no. 10, pp. 1009–1019, 1995.

[3] A. Zlotnick, I. Palmer, J.D. Kaufman, S.J. Stahl, A.C. Steven, and P.T. Wingfield, "Separation and crystallization of t = 3 and t = 4 icosahedral complexes of the hepatitis b virus core protein," *Acta Crystallogr D Biol Crystallogr*, vol. 55, no. Pt 3, pp. 717–720, 1999.

[4] K.A. Dryden, S.F. Wieland, C. Whitten-Bauer, J.L. Gerin, F.V. Chisari, and M. Yeager, "Native hepatitis b virions and capsids visualized by electron cryomicroscopy," *Molecular Cell*, vol. 22, no. 6, pp. 843–850, 2006.

[5] A.M. Roseman, J.A. Berriman, S.A. Wynne, P.J. Butler, and R.A. Crowther, "A structural model for maturation of the hepatitis b virus core," *Proc. of the Natl Acad of Sci USA*, vol. 102, no. 44, pp. 15821–15826, 2005.

[6] I.M. Sintorn, M. Homman-Loudiyi, C. Soderberg-Naucler, and G. Borgefors, "A refined circular template matching method for classification of human cytomegalovirus capsids in tem images," *Computer Methods and Programs in Biomedicine*, vol. 76, no. 2, pp. 95 – 102, 2004.

[7] M. Misiti, G. Oppenheim, J.M. Poggi, and Y. Misiti, *Wavelets and Their Applications (Digital Signal and Image Processing series)*, ISTE, 2006.

[8] R. Rangarajan, R. Venkataramanan, and S. Shah, "Image denoising using wavelets," .

[9] D. Donoho and I.M. Johnstone, "Adapting to unknown smoothness via wavelet shrinkage," *Journal of the American Statistical Association*, vol. 90, pp. 1200–1224, 1995.

[10] G. Farin, *Curves and surfaces for CAGD : a practical guide*, Morgan Kaufmann Publishers Inc., San Francisco, CA, USA, 2002.

[11] M. Pilu, A. Fitzgibbon, and R.B. Fisher, "Ellipse-specific direct least-square fitting," in *IEEE Int. Conf. on Image Processing*, September 1996, vol. 3, pp. 599–602.

[12] A. Fitzgibbon, M. Pilu, and R.B. Fisher, "Direct least square fitting of ellipses," in *IEEE Trans. Pattern Anal. Mach. Intell.*, May 1999, vol. 21, pp. 476–480.

[13] R.W. Zhou, C. Quek, and G.S. Ng, "A novel single-pass thinning algorithm and an effective set of performance criteria," *Pattern Recogn. Lett.*, vol. 16, no. 12, pp. 1267–1275, 1995.

[14] M. Couprie, "Note on fifteen 2d parallel thinning algorithms," Tech. Rep. GM 2006-01, Institut Gaspard Monge, 2006.

[15] J.B. Kruskal, "On the shortest spanning subtree of a graph and the traveling salesman problem," in *American Mathematical Society*, February 1956, vol. 7, pp. 48–50.

[16] M.D. Abramoff, P.J. Magalhaes, and S.J. Ram, "Image processing with imagej," *Biophotonics International*, vol. 11, no. 7, pp. 36–42, 2004.